Journal of Catalysis **203,** 157–167 (2001)
doi:10.1006/jcat.2001.3334, available online at http://www.idealibrary.com on IDEAL®

Transition-Metal-Substituted Titania-Loaded MCM-41 as Photocatalysts for the Degradation of Aqueous Organics in Visible Light

Lev Davydov, Ettireddy P. Reddy, Paul France, and Panagiotis G. Smirniotis[1]

Department of Chemical Engineering, University of Cincinnati, Cincinnati, Ohio 45221-0171

Received March 6, 2001; revised July 1, 2001; accepted July 1, 2001

Several transition metal (V, Cr, Fe)-substituted MCM-41-based specimens (Si/Me = 80) were synthesized by the incorporation of the transition metal during synthesis. They were then loaded with titania via sol–gel method and the photoactivity in visible light was explored. The XRD analysis showed the patterns of neat MCM-41 similar to those of siliceous MCM-41, while the loading of titania was in its amorphous form. The BET surface areas, however, were lower than those commonly found in siliceous MCM-41. This is due to the partial pore breakage, as recorded by the pore size distribution analysis. The transition metal dispersion found in the majority of the specimens studied was quite high (in the vicinity of 50%) and decreased with the loading of TiO_2. It was found that 25 wt% TiO_2 loaded on calcined Cr-Ti-MCM-41 and Cr-MCM-41 exhibits activity in visible light which is comparable with that demonstrated by commercial Degussa P25, utilizing UV light for the degradation of formic acid. The same catalyst in fully reduced form as well as titania-loaded chromium-silicon oxide of adequate composition did not show any activity. TiO_2/Fe-Ti-MCM-41 catalysts exhibited marginal activity for the degradation of formic acid. Similar vanadium-substituted catalysts (reduced and nonreduced) did not show any activity in visible light. These trends were also observed for the photodegradation of phenolic compounds in visible light, wherein the rates for 25% TiO_2/Cr-Ti-MCM-41 were significant. This behavior is essential for the development of photocatalysts which operate using solar light. A comparative DR UV–vis study showed the substantial absorption of visible light by all the catalysts employed. Furthermore, the coexistence of Cr^{3+} and Cr^{6+} in fully oxidized chromium substituted materials was detected (Cr^{3+}/Cr^{6+} ~0.25). Extensive TPR studies revealed a number of transitions in the titania-loaded transition-metal-substituted catalysts. In particular, the temperature of the transition $Cr^{3+} \rightarrow Cr^{2+}$ was found to considerably depend on the nature of chromium species in the MCM-41 matrix. This significantly contributes to the remarkable activity of TiO_2/Cr-Ti-MCM-41 and TiO_2/Cr-MCM-41, and this does not take place for both catalysts in their reduced form. Moreover, this transition is not present in the spent catalyst, which may be one of the possible reasons for deactivation. The surface composition of the most active catalyst was analyzed by XPS and showed considerable diffusion of chromium ions to the surface upon loading of titania. Two separate surface electronic levels were also found for TiO_2/Cr-Ti-MCM-41, corresponding to Si-O-Cr and Ti-O-Cr regions. Such an arrangement creates an opportunity for a two-step excitation of titania by two photons in the visible range. The proposed route of the catalytic activity of the above material in visible light involves the reaction of dopant level electrons with surface Cr^{6+}, which makes available valence band holes to perform oxidation reactions.

Key Words: **photocatalysis; MCM-41; visible light; doping; transition metal; sensitization.**

INTRODUCTION

Photooxidation by irradiated semiconductors is a relatively new technique of pollution abatement. The vast majority of current studies employ TiO_2 as the semiconductor due to its stability and relatively low price. However, it requires UV light to be excited and become capable of photooxidation. Ultraviolet radiation is expensive as it requires additional sources of energy, and it is also harmful to living species. Therefore, there is an urgent need to develop new photocatalysts capable of working in visible light. There are a number of semiconductors that can serve as candidates for this application. Cadmium sulfide has been studied for the photodegradation of organics in visible light, but its stability is very low due to photocorrosion and release of toxic cadmium ions into the reaction medium (1). Many oxides of transition metals absorb part or all of the spectrum of visible light. Colloidal iron (III) oxide was found to be active for the photooxidation of salicylic acid and phenol in visible light (2, 3), and leaching of iron ions was observed. Modified tungsten (VI) oxide was found active for the photodegradation of oxalic acid in visible light (4), but the rates reported are very low. Modified titanium dioxide was also explored for the degradation in visible light. Being doped with transition metals, TiO_2 exhibits better absorption response in the visible part of the spectrum. It was found (5) that dopants considerably reduce the activity of titania since they act as charge carrier recombination centers. Titania having iron (III) oxide deposited on its surface has also been prepared, and it was found that up to a certain content it increases the activity of TiO_2 in UV. Copper oxide (II) encapsulated

[1] To whom correspondance should be addressed. Fax: (513) 556-3473. E-mail: panagiotis.smirniotis@uc.edu.

0021-9517/01 $35.00

in titania was reported (6) to be active for the photooxidation of ethanol in visible light. However, the catalyst was preirradiated in UV, thus making unclear the true source of activity.

Overall, there has been no catalyst prepared for work in the visible light, which would combine chemical stability and high activity. Xu and Langford (7) reported an activity enhancement of titania when it was loaded onto zeolitic or mesoporous silica support. Transition-metal-substituted zeolites and MCM-41 have been synthesized previously (8). Substituting silicon with another atom during synthesis of MCM-41 makes it possible to atomically disperse the transition metal in the framework of the zeolite (9) under the action of the template. This property is used in the present study of titania-loaded transition-metal-substituted MCM-41 molecular sieves as potential photocatalysts for the oxidation of organics in visible light (10). Successful photooxidation in visible light can allow for more effective utilization of solar energy.

EXPERIMENTAL

Synthesis

Transition-metal-substituted MCM-41 supports with Si/Me = 80 and Si/Ti = 40 were synthesized as previously reported (9, 11) using Ludox HS-40 (DuPont) as the source of silica. The precursors used for the incorporation of transition metal oxides in the framework of MCM-41 were vanadia, $VO(C_3H_7O)_3$ (Alfa); chromia, $CrCl_3$ (Fisher); iron (III) oxide, $Fe_2(SO_4)_3$ (Fisher); and titania, titanium isopropoxide (Aldrich). All samples were prepared in the presence of hexadecyltrimethylammonium bromide (Fluka) as a template. The following is the typical preparation procedure: 35 g of Ludox was added to 14.55 mL of water under stirring, and 18.2 mL of 40% tetramethylammonium hydroxide (Fluka) was added. Independently, 18.25 g of the template was dissolved in 33 mL of water, and subsequently 7 mL of 28% NH_4OH was introduced. Finally, the above two solutions containing Ludox and template were mixed together. The corresponding amounts of each transition metal oxide precursor dissolved in either ethanol or water (depending on the nature of the precursor) were added dropwise from a pipette to the resulting mixture. The final mixture was stirred for 30 min and then transferred into polypropylene bottle and treated under autogenous pressure without stirring at 90–100°C for 3 days. The resulting solids were filtered, washed, dried, and calcined at 550°C for 10 h under air flow. The temperature profile was 2°C/min up, 15°C/min down.

The resulting catalyst (typicaly 1.5 g) was dispersed in ∼100 mL of isopropanol, and titanium isopropoxide was added to achieve 25% loading. The system was dried while stirring at ambient temperature. It was then placed in the oven to dry at 100°C for 1 h. The powder was then transferred into a boat-like crucible and calcined at 450°C for 3 h with a temperature ramp of 2°C/min.

Certain samples of Cr-MCM-41 and V-MCM-41 underwent reduction in hydrogen at 380°C. The temperature was chosen to avoid the formation of extraframework crystalline chromia (12). In this procedure, hydrogen (Wright Brothers, 99.9%) was run through a tubular reactor with a bed of catalyst with a heating rate of 2°C per minute and stay of 3 h at the final temperature.

Characterization

All catalysts were characterized using Nicolet powder X-ray diffractometer equipped with a CuK_α source to assess their crystallinity. MCM-41 powders were run from 2° to 7° (2θ) to assess the crystallinity of the matrix and from 20° to 50° to assess the crystallinity of the TiO_2 loading. Furthermore, the powders were characterized by UV–vis spectrophotometer (Shimadzu 2501PC) with an integrating sphere attachment ISR1200 for their diffuse reflectance in the range of wavelengths of 200 to 800 nm. $BaSO_4$ was used as the standard in these measurements. BET and pore size distribution studies were also conducted (using Micromeritics ASAP-2010 apparatus) to characterize the synthesized photocatalysts. The valence states of transition metal ions inside the solids were deduced from the diffuse reflectance spectra of the powders.

Temperature programmed reduction (TPR) experiments were carried out in a gas flow system equipped with a quartz microreactor, using a custom-made setup attached with a TCD detector. Approximately 100 mg of sample was pretreated in 23 mL/min flowing of He at 350°C for 1 h. After pretreatment, the catalyst samples were tested in 6 vol% H_2/He, 25 cm^3/min, and increasing the temperature from 100 to 800°C at 5°C/min and kept the temperature at 800°C for 2 h. The amount of hydrogen consumed by the catalyst sample in a given temperature range (in μmol/g) was calculated by integration of corresponding TCD signal intensities taking in account calibrated values obtained in separate experiments.

X-ray photoelectron spectroscopy was used to analyze the atomic surface concentration on Cr-Ti-MCM-41 and 25%TiO_2/Cr-Ti-MCM-41. The XPS analyses were conducted on a Perkin-Elmer Model 5300 X-ray photoelectron spectrometer with MgK_α radiation at 300 W. Typically, 89.45- and 35.75-eV pass energies were used for survey and high-resolution spectra, respectively. The effects of the sample charging were eliminated by correcting the observed spectra for a C 1*s* binding energy values of 284.5 eV. The powdered catalysts were mounted onto the sample holder and were degassed overnight at room temperature and pressures on the order of 10^{-7} Torr. The binding energies and atomic concentrations of the catalysts were calculated

via the XPS results using the total integrated peak areas of the Cr 2*p*, Ti 2*p*, Si 2*p*, and O 1*s* regions.

Photocatalytic Experiments

The photocatalytic testing included the degradation of organic compounds, which was performed in a batch-type round flat-plate reactor (Fig. 1) using a 200-W medium pressure mercury lamp (Ace Glass) as the light source. A 0.25-inch-thick Plexiglas filter (US Plastics, Catalog No. 44673) was utilized for the purpose of excluding ultraviolet radiation when conducting visible-light experiments. The cooling jacket around the reactor allowed to effectively preclude the IR part of the spectrum from penetrating into the reaction solution and cooled the lamp. The emission spectum of the lamp (obtained from the manufacturer) as well as the transmission spectrum of the filter (obtained spectrophotometrically) are presented in Fig. 2. Several reactants were tested for the photocatalytic degradation: 2,4,6-trichlorophenol (Fisher), chlorophenol (Aldrich), formic acid (Fisher). Although other researchers (5) used oxalic acid as their probe molecule for photodegradation, the choice of our reactants was justified by the possibility of the leaching of transition metal ions from the catalysts into the solution. Thus, to minimize such leaching, chemicals that cannot act as chelates were chosen. Prior to the reaction 0.5 L of the slurry (0.5 g/L of solids, 1 mM of the corresponding phenolic compound, pH 6, or 10 mM of formic acid, pH 4) was ultrasonicated for 10 min in an ultrasonic bath in order to assure the breakage of catalyst aggregates. The suspended catalyst in aqueous system was oxygenated (Wright Bros, 99.9%) at 0.5 L/min to assure the complete saturation. The temperature in the reactor

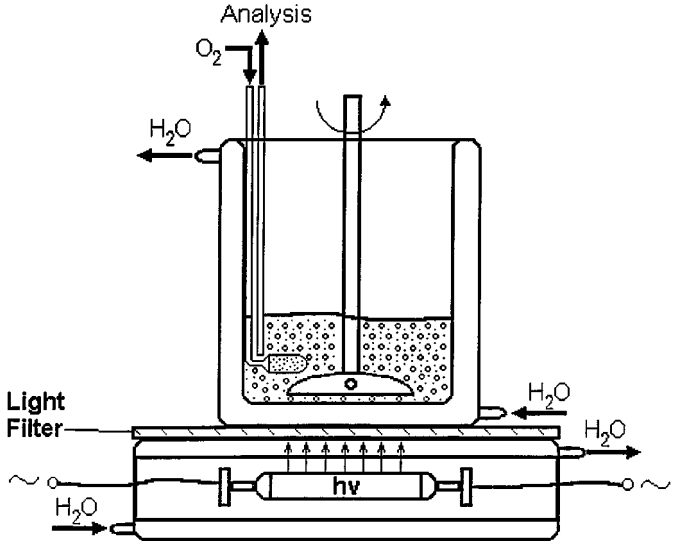

FIG. 1. Scheme of the photocatalytic reactor employed in the present study.

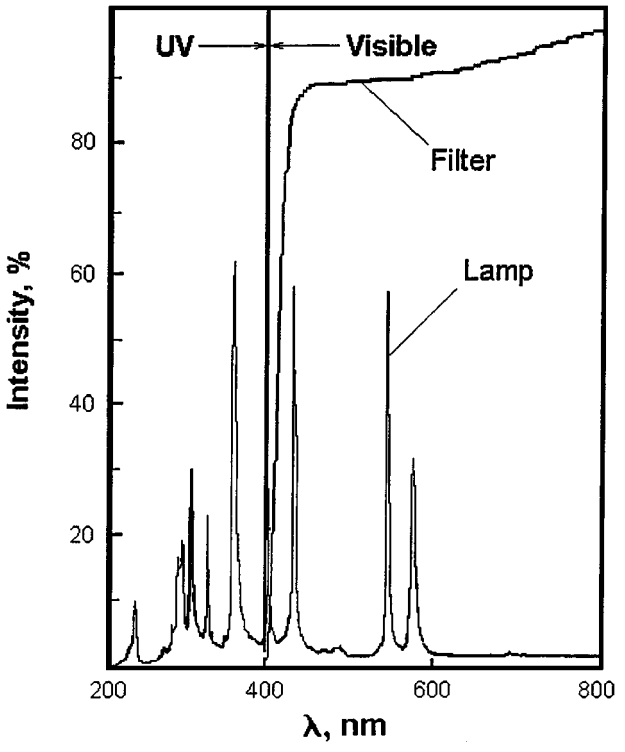

FIG. 2. Emission spectrum of the mercury lamp and transmission spectrum of the light filter.

was kept constant at $25 \pm 3^{\circ}$C. The concentration of phenol in the reactor was monitored by UV–vis spectrophotometry (Shimadzu PC2501) at the wavelength of 270 nm, the concentration of chlorophenol—at the wavelength of 274 nm. The concentration of 2,4,6-trichlorophenol was measured chromatographically (GC HP 6891 equipped with an FID), as described elsewhere (13). The concentration of formic acid was tracked using a conductivity meter (VWR Scientific, cell constant 10 cm^{-1}). The latter device was precalibrated for the measurements by standard solutions of formic acid. The presence of transition metal ions in the solution was also monitored by absorption spectrophotometry: Cr^{6+} at 374 nm, Cr^{3+} at 460 nm, Fe^{3+} at 304 nm, and V^{5+} at 436 nm. Standard solutions of $(NH_4)_2CrO_4$ (Fisher), $CrCl_3$ (Fisher), $FeCl_3$ (Aldrich), and NH_4VO_3 (Aldrich), respectively, were used for calibration purposes.

RESULTS AND DISCUSSION

The X-ray diffraction (XRD) analysis emloyed to characterize the crystallinity of the catalysts showed a number of trends. First, the diffractograms recorded from 2° to 7° (Fig. 3) exhibited the same location of peaks as siliceous MCM-41 (11). However, the intensities of these peaks are lower than those found for siliceous MCM-41. This can be attributed to the presence of foreign ions in the gel

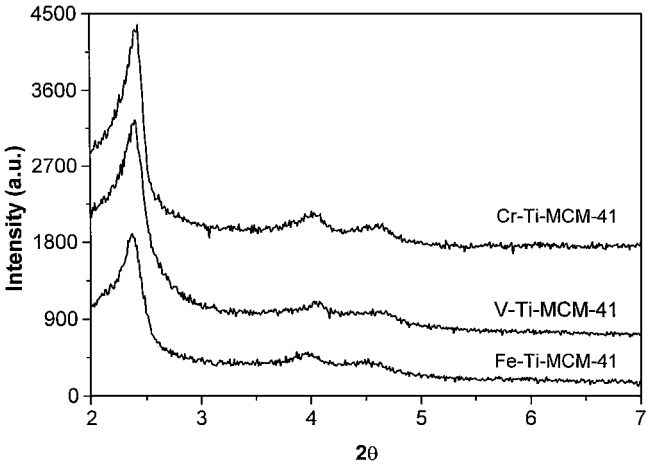

FIG. 3. XRD diffractograms of Me-Ti-MCM-41 (Si/Me-80, Si/Ti = 40) supports.

during synthesis, which can hinder the structure-directing action of the template by changing the ionic strength of the gel. A similar trend (the lowering of peak intensities) was observed by Kevan *et al.* (19). The second part of the XRD analysis was performed in the range of 20° to 50° in order to assess the crystallinity of TiO_2 loaded onto the transition metal substituted MCM-41 support. It showed that our samples exhibit low crystallinity of titania. Xu and Langford (7) observed a different trend when loading titania onto siliceous MCM-41. However, they utilized a different support (unmodified MCM-41) and different loading method (sol–gel precipitation with acid peptization). There are steric hindrances associated with the formation of titania clusters inside zeolites and mesoporous molecular sieves (7) due to the low pore size of these materials. This does not allow for the efficient crystal growth under the calcination conditions employed, and the overall crystallinity of TiO_2 in our samples remains low. It is also worth noting that no peaks corresponding to the transition metal oxides (those of V, Cr, and Fe) were observed on our diffractograms. This indicates that our oxides were either atomically dispersed in the framework of MCM-41 or attained an amorphous form outside the framework. Transition metal ions are expected to be in intimate contact with the loaded titania, provided that uniform distribution of titania on the pore walls of the molecular sieve has been achieved. With this structure it will be possible to combine the effect of TiO_2 and the atomic dispersion of the transition metal inside MCM-41 achieved as a result of the work of a structure-directing agent. This is not possible for mixed oxides. It is expected that this special arrangement will yield increased activity for the photodegradation of aqueous organic pollutants in visible light.

The Fourier Transform Infrared (FTIR) spectra (not shown) of the three types of the powders (MCM-41, Cr-Ti-MCM-41, and TiO_2 loaded Cr-Ti-MCM-41) were recorded in the range of wavenumbers of 400–4000 cm^{-1} in order to assess the trace amounts of the partially decomposed surfactant template remaining inside the MCM-41 material. We observed similar trends for all three materials with different intensities of the transmission peaks. The presence of a peak at about 1620 cm^{-1} for all MCM-41 materials clearly shows the presence of quaternary ammonium salts. The second calcination allows to remove the template and chemisorbed ammonia (1850 cm^{-1}).

The BET surface areas (SA), peak pore sizes (PPS), and oxygen chemisorption results (% of metal dispersion, MD) are summarized in Table 1. One can observe that the presence of transition metal ions in the gel during synthesis lowers the SA of the resulting MCM-41 material (for example, SA = 941 m^2/g for siliceous MCM-41 and SA = 703 m^2/g for Cr-Ti-MCM-41). Nonetheless, the BET surface area of the catalysts employed in the present study is much higher than titanias conventionally used for UV-assisted heterogeneous photocatalysis (14). The PPS also changes with the introduction of the transition metal. Since the same surfactant template was utilized for the synthesis of both siliceous and transition-metal-substituted MCM-41 materials, one should expect to obtain PPS in a close range for both types of catalysts. The above discrepancy is therefore due to the partial breakage of the tubular walls of the MCM-41 structure. The presence of transition metal salts changes the ionic strength of the gel during synthesis, which may hinder the action of the template and result in the formation of bigger pores (as well as lower SA).

Moreover, some loss of SA is observed when titania is deposited on the MCM-41 support, as the pore diameters are expected to decrease (Table 1). This is a logical conclusion

TABLE 1

BET Areas, Peak Pore Sizes, and Metal Dispersions of the Catalysts Used in the Present Study

Catalyst	BET SA (m^2/g)	Pore volume (cm^3/g)	Peak pore size (nm)	% of metal dispersion[a]
MCM-41	941	0.94	4.2	Not defined
25%TiO_2/MCM-41	667	0.56	3.4	0.1
Cr-Ti-MCM-41	702	1.1	6.7	51.0
25%TiO_2/Cr-Ti-MCM-41	571	0.67	5.1	23.4
Cr(III)-imp. MCM-41	1217	1.0	4.3	51.8
25% TiO_2/Cr(III)MCM-41	932	0.69	2.7	34.2
CrSiOx	553	0.66	4.7	74.5
25% TiO_2/CrSiOx	425	0.41	4.1	195.3[b]
Fe-Ti-MCM-41	719	0.78	5.7	28.6
25%TiO_2/Fe-Ti-MCM-41	536	0.68	5.1	37.8
V-Ti-MCM-41	742	1.3	7.1	17.7
25%TiO_2/V-Ti-MCM-41	628	0.63	3.9	14.4

[a] Metal surface area, determined by oxygen chemisorption, stoichiometric factor metal to oxygen equals to 1.

[b] Cr is present in the oxidation state of +6 (CrO_3). Therefore, metal dispersion is over 100% because the actual metal to oxygen ratio is 1 : 3.

of the loss of surface area due to partial blockage of the pores. Comparing the Cr-substituted MCM-41 samples elucidates the following phenomena. Smaller percentages of titania deposition (∼10%) led to an almost negligible (∼1%) loss of the SA. On the contrary, higher coverages (25%) lead to substantial losses in the SA (∼15%). This clearly indicates that the distribution of titania in the two samples is different. Low loadings lead to layer-type distribution of titania (7), which simply covers the pore walls. Higher loadings fill up some of the pores leading to their partial blockage, such that the removal of isopropyl alcohol upon calcination does not open the pore mouth.

The results of oxygen chemisorption (percentage of metal dispersion, MD) are also presented in Table 1. Naturally, no MD has been observed for the siliceous MCM-41 sample as well as that containing 25% of TiO_2. However, all transition-metal-substituted MCM-41 materials exhibited strong oxygen chemisorption. The greatest MD was observed for chromium-incorporated samples, followed by iron- and vanadium-incorporated ones. One can also observe that the MD of chromium in Cr-Ti-MCM-41 is comparable with that of Cr(III)-impregnated MCM-41 and greater than that in the mixed chromia–silica. The former is due to the higher SA of the siliceous MCM-41 (which leads to significant dispersion capacity), and the latter can be attributed to the presence of individual clusters in the mixed oxide. The oxygen chemisorption results also show a pronounced effect of the TiO_2 loading on the MD. For chromium-incorporated and -impregnated MCM-41 samples, about 50 and 35%, respectively, of the MD is lost upon loading 25% of titania; the loss of MD is lower for V-Ti-MCM-41. This is due to partial blockage of the transition metal sites by the TiO_2 loading, making them inaccessible to oxygen. It should be noted that Cr-MCM-41, as well as TiO_2/Cr-MCM-41, exhibited exactly the same trends in spite of the lack of titanium atoms in the framework.

The dispersion of chromium in the mixed chromia–silica significantly increases upon the loading of titania. This is because the clusters of chromia (VI) in the mixed amorphous oxide can disperse in the titania precursor during loading, which is further enhanced by calcination. As a result, we obtain values of MD over 100%, which is an overestimation due to the use of the stoichiometric ratio of oxygen to metal equal to one. Contrary to Cr- and V-, Fe-Ti-MCM-41 exhibits higher MD of iron on titania than inside and on the surface of MCM-41, as the oxygen chemisorption is higher for the TiO_2 loaded sample. This hints at low amounts of Fe^{3+} in the framework of MCM-41, which was also found by others (15).

For the photocatalytic testing of the catalysts specified, several modifications of the conventional reactor setup were necessary. More specifically, one needs to assure that only visible light reaches the catalyst suspension. The transmission spectrum of the filter exhibits a sharp decrease at 400 nm, thus effectively eliminating the ultraviolet part of the spectrum (Fig. 2). Considering that all of our catalysts absorb light significantly below 550 nm, the two strong bands of the mercury lamp available for the reaction are 405 and 435 nm. In order to have a quantitative means of comparison, the photodegradation of the respective reactants on UV-irradiated Degussa P25 powder and visible-irradiated Degussa P25 was undertaken as well. The results are shown in all figures depicting the course of degradation (Figs. 4–6). Moreover, catalysts without loading of titania (neat V-Ti-MCM-41, Cr-Ti-MCM-41, and Fe-Ti-MCM-41) were tested for the photodegradation of formic acid and yielded no discernible activity. All reaction solutions were tested for the leaching of transition metal ions. It is remarkable to note that the leaching was negligible for all TiO_2 loaded catalysts, and it was considerable for the neat chromium substituted MCM-41 materials (see below).

The time course of the photodegradation of formic acid on visible-light irradiated catalysts is shown in Fig. 4. Nonreduced (as calcined) chromium substituted MCM-41 with loaded titania did exhibit activity comparable with that of Degussa P25 in UV (Fig. 5). For the TiO_2/Cr-Ti-MCM-41 the concentration of formic acid decreases steadily for about 60 min and then levels off at approximately 25% of conversion. This behavior is unexpected, since from a physics point of view the altervalent cations (especially with

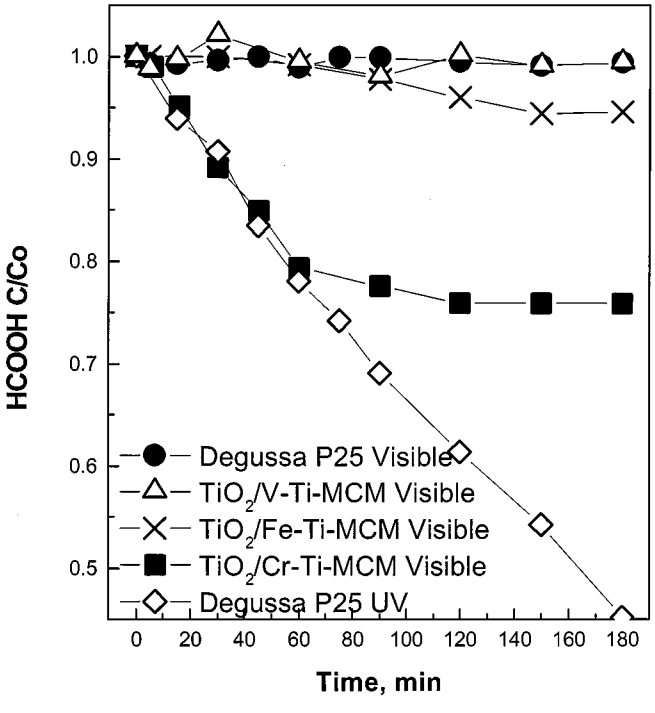

FIG. 4. Time course of the degradation of formic acid on the V-, Cr-, and Fe-substituted catalysts (Table 1). Degussa P25 in UV is shown for comparison (pH 4, $T = 25 \pm 3°C$, catalyst concentration—1 g/L).

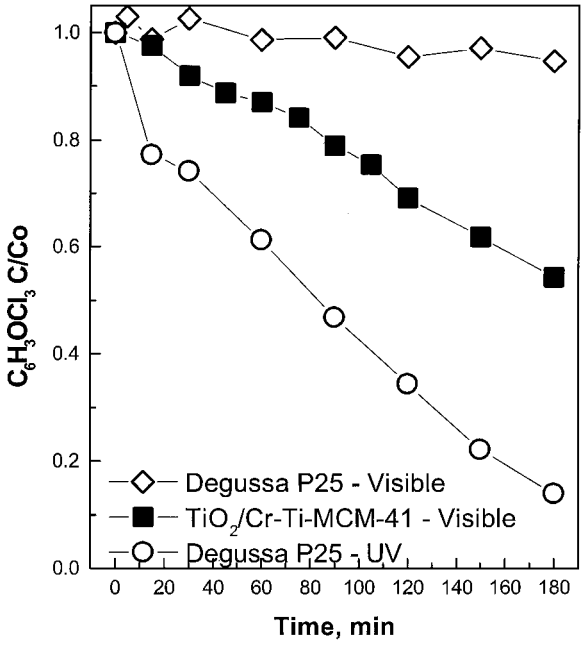

FIG. 5. Time course of the degradation of 2,4,6-trichlorophenol on the Cr-substituted catalyst of Table 1. Degussa P25 in UV is shown for comparison (pH 6, $T = 25 \pm 3^{\circ}$C, catalyst concentration—1 g/L).

the oxidation state of 5+) would serve best as dopants (16), but we will see later that the primary doping species in the above catalysts is Cr^{6+}. Iron substituted MCM-41 sieves loaded with titania also exhibit some photoactivity (Fig. 4). The concentration of formic acid monotonically decreases and levels off at about 6% of conversion, which was proved

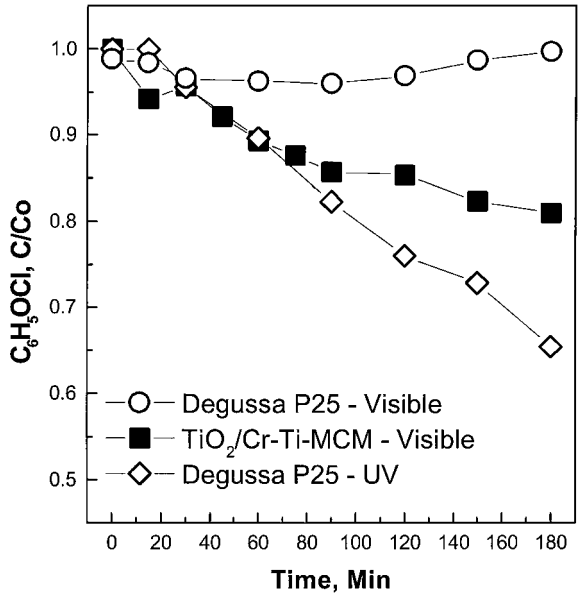

FIG. 6. Time course of the degradation of 4-chlorophenol on the Cr-substituted catalyst of Table 1. Degussa P25 in UV is shown for comparison (pH 6, $T = 25 \pm 3^{\circ}$C, catalyst concentration—1 g/L).

in three independent experiments. The maximum degradation rate is considerably lower than that of neat titania (P25) in UV. Such behavior can be explained on the basis of the structure of neat Fe-Ti-MCM-41. It was found (8) that the majority of iron oxide is located outside the framework of MCM-41. This makes possible the contact of iron oxide (and not iron ions in the framework) with titania. It is known, however, that the presence of neat iron oxide (III) is deleterious for the activity of the titania-based mixed oxide photocatalysts in visible light (17). The activity of TiO_2/V-Ti-MCM-41 was explored under identical operation conditions (Fig. 4). However, no discernible conversion of formic acid under visible light was detected.

Several other materials were prepared and tested for the photodegradation of formic acid for comparison purposes. The first group included TiO_2/V-Ti-MCM-41 and TiO_2/Cr-Ti-MCM-41, but now both photocatalysts were reduced in hydrogen. No activity was observed, which was also the case for the same nonreduced vanadium-substituted catalyst. The second group of materials was synthesized to compare directly with the most active catalyst, namely, the nonreduced TiO_2/Cr-Ti-MCM-41. In particular, siliceous MCM-41 was impregnated with CrO_3, $Cr(NO_3)_3$, and a mixed chromium–silicon oxide was also synthesized to achieve the ratio of Si/Cr equal to 80. None of these test materials, however, exhibited any meaningful activity for the photodegradation of formic acid in visible light. Therefore, the considerable photoactivity of nonreduced TiO_2/Cr-Ti-MCM-41 is due not only to the presence of chromium ions and titania, but also to the special environment provided by the MCM-41 matrix.

The performance of the most active catalyst (TiO_2/Cr-Ti-MCM-41) was also tested for the photodegradation of phenolic compounds in visible light. As seen from Fig. 5, the above specimen exhibits photoactivity to decompose 2,4,6-trichlorophenol. This is also the case for 4-chlorophenol (Fig. 6). The activity for the degradation of these reactants in visible light is not as high as that of Degussa P25 in UV. As in the case of Degussa P25, the activity acquires lower values with the smaller number of chlorine atoms in the reactant molecule, primarily due to the lesser generation of secondary active chlorine radicals (18). No deactivation is observed for the above two reactions in visible light, contrary to the photodegradation of formic acid. Apparently, the chlorine atoms help to reactivate the catalyst. It should be also noted that the incorporation of titanium during synthesis did not play any role in the photocatalytic activity of the above materials. More specifically, TiO_2/Cr-Ti-MCM-41 was equally active with TiO_2/Cr-MCM-41. Therefore, the interaction of chromium and titanium in the framework of MCM-41 is not essential for the photocatalytic activity in visible light.

Three characterization techniques, namely, diffuse reflectance UV–visible spectroscopy (UV–vis), temperature-

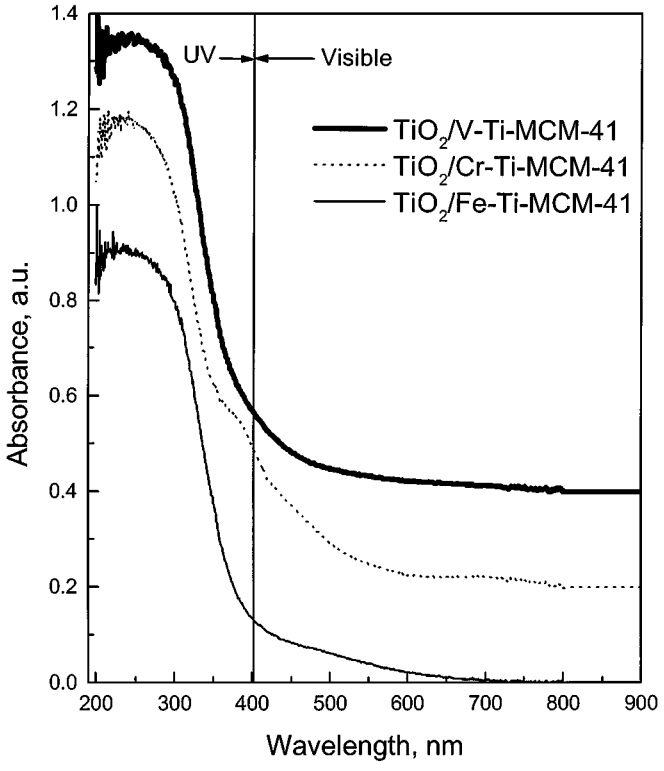

FIG. 7. UV–vis diffuse reflectance spectra of the titania-loaded, transition-metal-substituted photocatalysts (titania loading—25 wt%).

programmed reduction (TPR), and X-ray photoelectron spectroscopy (XPS) were utilized in an attempt to elucidate the reasons of the remarkable activity of TiO_2/Cr-Ti-MCM-41 for the photooxidation in visible light.

One can observe that the photocatalysts employed in the present study (Fig. 7) drastically differ from neat titanium dioxide (not shown). Their absorption edges are in the vicinity of 500–600 nm, thus shifting the bandgap position to ∼2.0 eV. This justifies why these photocatalysts can be potentially good candidates for performing photochemical reactions in visible light. It should be noted that the enhanced absorption of the composite catalyst is a necessary condition for the photoactivity in visible light, but not sufficient for its ability to perform photocatalytic reactions in visible light, as was observed in the activity studies above. The upper branch of the curves (200–350 nm) practically coincides with that of titania. Then, the absorption by titania itself sharply decreases, and the absorption of light in the range of 350 to 450 nm is exhibited by the heterojunction of titania with the corresponding transition metal incorporated in MCM-41. The absorption after 450 nm is probably due to the transition metal oxide itself. It should be noted that we have chosen to analyze 25 wt% loaded composites as to assure that the presence of a large quantity of the second oxide (TiO_2) does not overshadow the true optical properties in visible light.

Iron-substituted MCM-41 samples behave differently from vanadium-substituted ones (Fig. 7). The loading of titania shifts the absorption edge by about 100 nm toward UV. While the spectrum of V-substituted specimen is monotonic, that of an Fe-substituted specimen exhibits a shoulder in the range of 400–500 nm. Its position and shape is similar to that found in mixed oxides (17) and different from pure TiO_2 or Fe_2O_3. When considering Cr-Ti-MCM-41-based samples (Fig. 7), the situation is some what similar to the prior work. It was found previously (19) that there are three species inside Cr-substituted MCM-41: framework Cr^{3+}, extraframework Cr^{3+}, and extraframework Cr^{6+}. Such comparison also allows to attribute the peaks of Cr-Ti-MCM-41 at 275 and 370 nm to Cr^{6+} and shoulder at ∼475 nm to Cr^{3+} similar to that seen in the previous study (20). Neat Cr-Ti-MCM-41 exhibits absorption maximum at ∼390 nm which corresponds to Cr^{6+} species. When loaded with titania, this maximum (corresponding to Cr^{6+}) is overshadowed by the absorption by TiO_2, leaving only an absorption shoulder. Finally, the reduced sample of titania-loaded Cr-Ti-MCM-41 (inactive) does contain a small remainder of the above maximum. This can be attributed to incomplete reduction of Cr^{6+} species. It was found (20) that some of the Cr^{6+} species inside Cr-Ti-MCM-41 are nonreducible. The reduced form of 25% TiO_2/V-Ti-MCM-41 also exhibited enhanced absorption of visible light, but lacked any photoactivity.

In order to determine the ratio of Cr^{6+} to Cr^{3+} in our calcined Cr-Ti-MCM-41 samples, a leaching experiment was performed, and the presence of chromium ions in the powders and in solution was monitored spectrophotometrically. The disappearance of Cr^{6+} was observed, while Cr^{3+} was retained by the material. The amount of Cr^{6+} leached in two independent experiments constituted about 80% of the chromium introduced during synthesis. Therefore, the majority of Cr^{3+} oxidized to Cr^{6+} during the calcination of Cr-Ti-MCM-41. This again testifies for the high dispersion of chromium inside MCM-41, since it is impossible to obtain Cr^{6+} by calcination of common chromium (III) salts (21). Furthermore, no leaching of Cr^{3+} could be detected spectroscopically. Similar leaching tests were performed on the most active catalyst, TiO_2/Cr-Ti-MCM-41, and no significant leaching was detected. Conclusively, the UV–vis study allowed to reveal the coexistence of Cr^{3+} and Cr^{6+} inside MCM-41, which contributes to its special photocatalytic behavior.

Temperature-programmed reduction (TPR) was used in the present study to investigate different oxidation states of the transition-metal-substituted MCM-41 materials and relate these oxidation states with the photocatalytic performance. Figure 8 compares the TPR profiles for a number of Cr-containing materials. One can observe that the reduction behavior is almost identical. Two major peaks can be found: 440°C (corresponds to $Cr^{6+} \rightarrow Cr^{3+}$, according

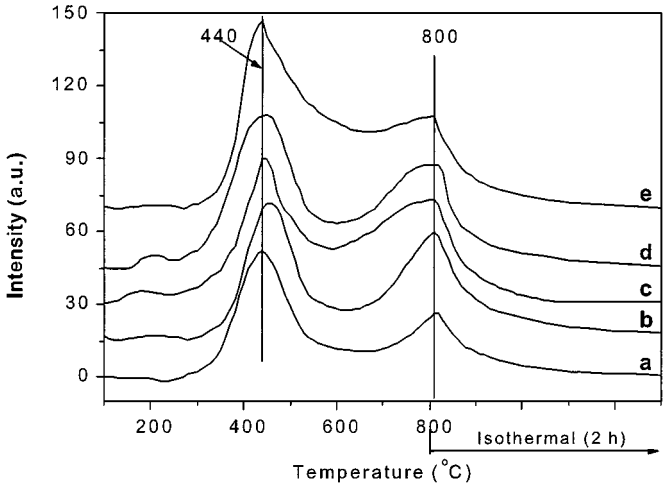

FIG. 8. TPR profiles of catalysts: (a) $(Cr(NO_3)_3$ on MCM-41; (b) CrO_3 on MCM-41; (c) Cr-Ti-MCM-41; (d) Cr–Si mixed oxide; (e) Cr-MCM-41.

to (22)) and ∼800°C. The first peak validates our earlier observations by UV–vis about the presence of Cr^{6+} in the MCM-41 based materials made with Cr(III) precursor. The second peak was observed even in siliceous MCM-41, so it can be attributed to the hydroxyl groups leaving the surface of amorphous silica. When TiO_2 is loaded onto our Cr-containing materials, the TPR profiles show marked difference (Fig. 9). We still observe the two major peaks at 440° and 800°C, but a shoulder appears before the first peak and another peak appears between them. The shoulder in the range of 250–350°C corresponds to the dehydroxylation of TiO_2 surface. The position of the new peak is apparently due to the transition $Cr^{3+} \rightarrow Cr^{2+}$ (23). It should be noted that the position of this new peak

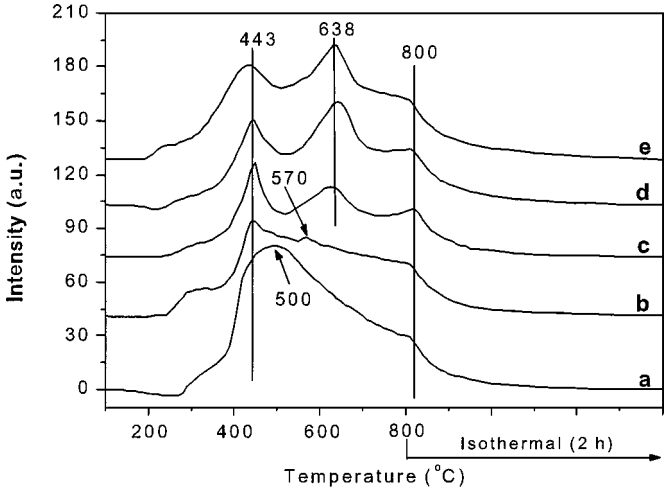

FIG. 9. TPR profiles of 25 wt% TiO_2-loaded catalysts: (a) Cr-MCM-41; (b) Cr-Ti-MCM-41; (c) $(Cr(NO_3)_3$ on MCM-41; (d) CrO_3 on MCM-41; (e) Cr–Si mixed oxide.

strongly depends on the preparation method. For the titania-loaded, chromium-impregnated MCM-41 materials (the top three curves of Fig. 9), the peak is located at about 640°C. For TiO_2/Cr-MCM-41 and TiO_2/Cr-Ti-MCM-41 this peak is much less pronounced and shifted by about 70°C toward the lower temperatures. The position of the central peak corresponding to the $Cr^{3+} \rightarrow Cr^{2+}$ transition is at 520°C (found by deconvolution), which is considerably lower than the reduction temperature recorded by other researchers (23). Apparently, highly dispersed Cr^{3+} (Cr^{6+} reduces at 440°C) inside MCM-41 facilitates the above transition, contrary to the behavior of the materials simply impregnated with chromium precursors (TiO_2/Cr(III)-imp MCM-41, TiO_2/Cr(VI)-imp MCM-41) or amorphous silica–chromia. Since the composition of all the materials in Fig. 9 is the same, the lower temperature of the reduction of titania is due to a high degree of its interaction with the framework chromium. Furthermore, when incorporated into MCM-41 during synthesis, chromium is expected to attain the tetrahedral coordination (19), while the impregnated MCM-41 has chromium in its native coordination. This may also contribute to the special interaction of chromium and titanium oxides in our active catalysts for the photodegradation of aqueous organic pollutants in visible light.

The TPR diagrams of spent chromium-based photocatalysts were also recorded. The qualitative TPR behavior of the inactive catalysts remained almost unchanged after the reaction. On the contrary, the peaks corresponding to the interaction of chromium and titania in the active catalyst have disappeared, and the TPR profile became similar to that of TiO_2/MCM-41. The disappearance of the interaction described is apparently the reason for the deactivation observed for this photocatalyst after 1 h of photocatalytic reaction with formic acid.

The samples of 25%TiO_2/Cr-Ti-MCM-41 and Cr-Ti-MCM-41 were investigated by X-ray photoelectron spectroscopy. The XPS bands of O 1*s*, and Cr 2*p* core levels are shown in Figs. 10 and 11, respectively. The binding energy values of O 1*s*, Si 2*p*, Ti 2*p*, and Cr 2*p* photoelectron peaks and Cr/Si and Cr/Ti surface atomic concentration ratios as determined by XPS of the above catalysts are summarized in Table 2. All these figures and Table 2 clearly indicate that the XPS peaks depend on the surface concentration of chromia in the Cr-Ti-MCM-41 and 25%TiO_2/Cr-Ti-MCM-41. The O 1*s* profile, as shown in Fig. 10, is due to the overlapping contribution of oxygen from silica and chromia in the case of Cr-Ti-MCM-41 and silica, chromia and titania in the case of 25%TiO_2/Cr-Ti-MCM-41, respectively. As shown in Fig. 10a and Table 2, from the deconvoluted XPS spectra of O 1*s* corresponding to 25%TiO_2/Cr-Ti-MCM-41, one can clearly detect that there are three types of O 1*s* peaks. Their binding energy values are at 529.6, 530.0, and 532.7 eV (Table 2) and belong to the oxygen atoms that are more

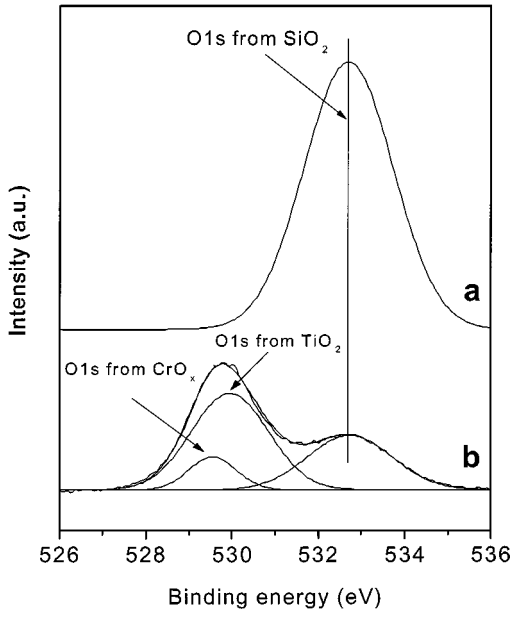

FIG. 10. Deconvoluted XPS spectra for O 1*s* peak: (a) Cr-Ti-MCM-41; (b) 25% TiO_2/Cr-Ti-MCM-41.

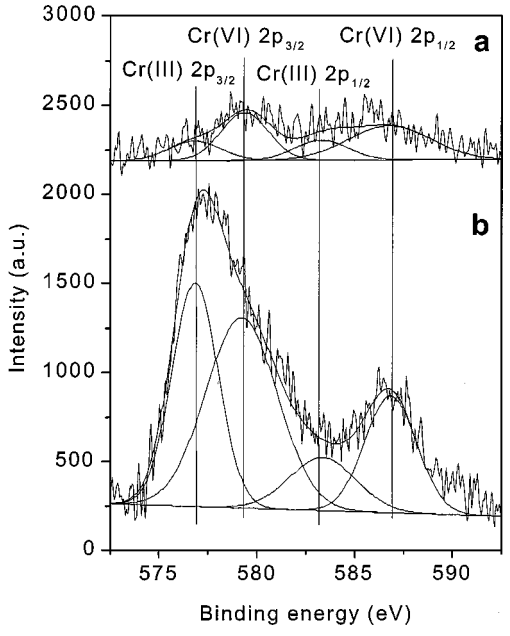

FIG. 11. Deconvoluted XPS spectra for Cr 2*p* peak: (a) Cr-Ti-MCM-41; (b) 25% TiO_2/Cr-Ti-MCM-41.

bound to Cr (CrO_x), Ti (TiO_2) (24) and Si (SiO_2) (25), respectively. The binding energy values of three different types of O 1*s* peaks can be judged from the difference in the electronegativity of the elements (26). It should be noted that only one oxygen photoelectron peak at 532.7 eV that belongs to SiO_2 was observed in the case of Cr-Ti-MCM-41. The peak intensity of O 1*s* XPS band corresponding to SiO_2 reduced drastically when titania was loaded on Cr-Ti-MCM-41. This clearly indicates that the titania loading on Cr-Ti-MCM-41 changes its structural behavior and also possible migration of oxygen atoms is taking place with respect to different structural modifications.

Table 2 lists the Cr/Si and Cr/Ti surface atomic concentration ratios for Cr-Ti-MCM-41 and 25% TiO_2/Cr-Ti-MCM-41. The ratio of the Cr/Si for Cr-Ti-MCM-41 is smaller than that of Cr/Si for 25% TiO_2/Cr-Ti-MCM-41. As a matter of fact, it was due to the surface coverage of titania and chromia segregation onto the surface of Cr-Ti-MCM-41. As shown in Fig. 11 and Table 2, the surface concentration of Cr 2*p* is more predominant in the case of 25% TiO_2/Cr-Ti-MCM-41 than in case of Cr-Ti-MCM-41, but the Cr(VI) peak at 579.3 eV is more dominant than Cr(III) in the latter case. XPS analysis shows two different Cr species or chemical states on the catalysts surfaces (see Fig. 11). The simple interpretation would be to assigned the lowest binding energy peak at 576.7 eV, corresponding to Cr(III), and the highest binding energy peak at 579.3 eV, corresponding to Cr(VI). The coexistence of Cr_2O_3 and CrO_3 has often been observed on different supports (27). An increase of the Cr(III)/Cr(VI) ratio is observed when the surface concentration of Cr increases (see Fig. 11). The enhancement of the surface mobility and surface rearrangement of chromia was due to the loading of 25% TiO_2 on Cr-Ti-MCM-41. The possible explanation for these data is the migration of extraframework chromium away from the TiO_2/Cr-Ti-MCM-41 interface. This type of structural modifications could occur and lead to variations in the dispersion. It could also reflect the heterogeneous character of the surface chromia,

TABLE 2

XPS Binding Energies for the Select Photocatalysts

	BE (eV)										Surface Atomic Ratios	
	Cr $2p_{3/2}$		Cr $2p_{1/2}$					O 1*s*				
Catalyst	6+	3+	6+	3+	Ti $2p_{2/3}$	Ti $2p_{1/2}$	Si 2*p*	CrO_x	TiO_2	SiO_2	Cr/Ti	Cr/Si
25% TiO_2/Cr-Ti-MCM-41	579.3	576.8	586.7	583.2	458.5	464.2	103.5	529.6	530.0	532.7	0.136	0.258
Cr-Ti-MCM-41	579.3	576.8	586.7	583.3	—[a]	—[a]	103.5	—[a]	—[a]	532.7	—[a]	0.0014

[a] Corresponding species not found on the surface of the catalyst.

which leads to the existence of two separated electronic levels as shown previously. Further confirmation was obtained by characterization of Cr-Ti-MCM-41 and 25% TiO_2/Cr-Ti-MCM-41 catalysts with UV–vis and photocatalytic degradation of organic pollutants.

In order to explain the promising activity of 25% TiO_2/Cr-Ti-MCM-41 for the visible light assisted photodegradation of organic contaminants it is helpful to generalize the surface characterization results described above. The negligible activity of vanadium-substituted catalysts is likely to be due to the low degree of interaction of the loaded titania with the V-Ti-MCM-41 matrix. Considering the absorption spectrum of the above catalyst (Fig. 7), one can observe that it is monotonic, thus lacking the absorption shoulders usually found in mixed oxides. This hints at the possibility of low interaction between the support and titania. The marginal activity of 25% TiO_2/Fe-Ti-MCM-41 is probably due to the lack of metal dispersion (Table 1), and as a result, the lack of the interaction with the loaded titania. Although the absorption of the latter catalyst contain the shoulders characteristic of mixed oxides (Fig. 7), it is very likely that iron oxide did not incorporate into the framework of MCM-41 (15). Therefore, the interaction between Fe-Ti-MCM-41 can exist, but the area of the heterojunction is insufficient to produce a significant effect.

When considering chromium-substituted catalysts, all the factors necessary for the photoactivity in visible light are present. There are absorption shoulders in the visible range (Fig. 7), high metal dispersion (Table 1), specific transition $Cr^{3+} \rightarrow Cr^{2+}$ (Fig. 9), and surface enrichment of chromium species upon the loading of titania (Fig. 11). Furthermore, from the XPS studies one can observe (Table 2) that some surface chromium is present in neat Cr-Ti-MCM-41 specimens. This can be attributed to extraframework chromium species. Therefore, two types of interactions are possible in TiO_2/Cr-Ti-MCM-41 or TiO_2/Cr-MCM-41, namely Cr-doped mesoporous SiO_2 (MCM-41) with TiO_2 and extraframework CrO_x with TiO_2. The projected structure of the above composite catalyst is presented in Fig. 12. It should be noted that the presence of tetrahedrally coordinated six-valent chromium of the catalyst is essential since its fully reduced form does not exhibit any photoactivity, as described above. The role of three-valent chromium, however, is still unclear since the deactivated catalyst was rich in Cr(III).

The latter phenomenon leads to a conclusion that Cr(VI) is the species primarily responsible for the photoactivity in visible light. Figure 13 explains the proposed mechanism of the charge generation happening at the heterojunction of the loaded titania with chromium-incorporated MCM-41. Chromium(VI)-doped glasses (28) as well as mesoporous silicas (29) are known for their tetrahedral coordination of chromium. Such coordination allows for a special transition under visible light: $Cr^{6+}{=}O^{2-} \rightarrow Cr^{5+}{-}O^{1-}$. Such a transition, when it happens in contact with amorphous TiO_2, can produce an effect similar to that found in platinum (IV) chloride modified amorphous titania (30). In particular, the Cr^{5+} species can possibly donate an electron into the surrounding TiO_2 and O^{-1} can scavenge an electron from the

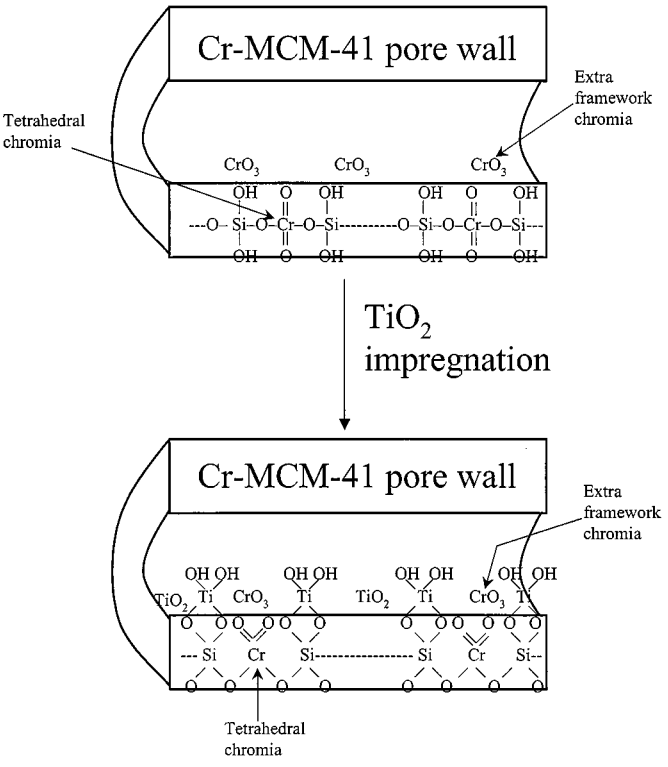

FIG. 12. The projected structure of titania-loaded transition-metal (example: chromium)-substituted MCM-41 photocatalysts: (top) neat Cr-MCM-41 material; (bottom) TiO_2-loaded Cr-MCM-41 material.

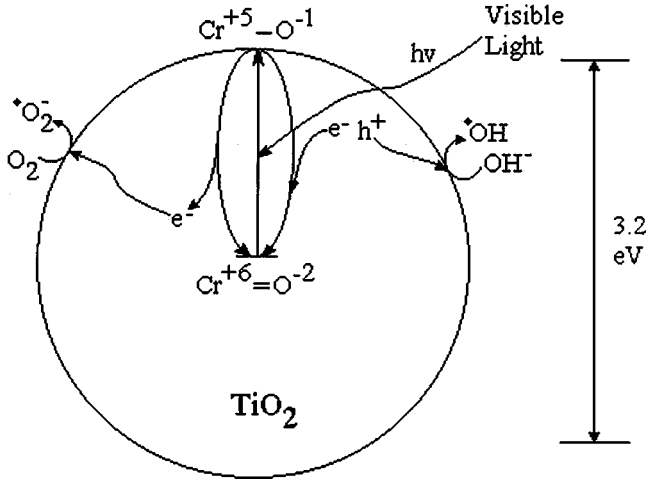

FIG. 13. Proposed mechanism of photooxidation and deactivation on TiO_2/Cr-(Ti)-MCM-41. Active Cr^{6+} species are incorporated in SiO_2 matrix.

surrounding TiO_2. In this case, the charge separation will occur, which will lead to a hole and an electron in TiO_2. If this process happens at or near the catalyst surface, the charges can interact with the surface hydroxyl groups or adsorbed oxygen to produce active oxygen radicals. As observed before, the photodegradation of certain test compounds leads to the deactivation of 25% TiO_2/Cr-Ti-MCM-41. Since the charge transfer to adsorbed oxygen is the limiting stage in photocatalysis (31), one can expect some accumulation of electrons on the surface of the catalyst. These electrons can possibly reduce Cr(VI) to Cr(III), which will lead to the depletion of the six-valent chromium and subsequent deactivation of the catalyst. In summary, the above mechanism is an attempt to clarify the mode of interaction between the amorphous titania and Cr-Ti-MCM-41 support. More information on the exact positions and coordinations of atoms is needed for this mechanism to be fully supported experimentally.

CONCLUSIONS

Several transition-metal-based, titania-loaded MCM-41 (Si/Me = 80, titania content—25 wt%) materials were tested for the degradation of organics in visible light. The chromium-substituted MCM-41 was found to serve as the best support for titania to achieve the highest degradation rates of formic acid, 2,4,6-trichlorophenol, and 4-chlorophenol. The change in the state of the catalyst during the reaction was observed for Cr-substituted molecular sieves, which led to its deactivation. The UV–vis spectrophotometric study revealed the coexistence of Cr(III) and Cr(VI) oxides inside the substituted MCM-41 at the ratio of 0.25. TPR showed the specific interaction of Cr and Ti in these materials, which is believed to contribute to their photocatalytic activity in visible light. XPS revealed increased surface concentrations of Cr ions upon the loading of TiO_2, which at the same time allows to minimize the leaching of chromium ions. The mechanism of the photodegradation in visible light on titania-loaded, transition-metal-substituted MCM-41 is proposed.

ACKNOWLEDGMENTS

The authors are grateful to the Young Investigator Award of the United States Department of Army (Grant DAAD 19-00-1-0399) and NATO Science for Peace Program (Grant SfP-974209) for their support of this work. The authors thank Procter and Gamble Corp. for their help to originate this work.

REFERENCES

1. Khairutdinov, R. V., *Colloidal J.* **59**, 535 (1997).
2. Pal, B., and Sharon, M., *J. Chem. Technol. Biotechnol.* **73**, 269 (1998).
3. Chatterjee, S., Sarkar, S., and Bhattacharya, *J. Photochem. Photobiol. A* **81**, 199 (1994).
4. Ashokkumar, M., and Maruthamuthu, P., *Int. J. Hydrogen Energy* **16**, 591 (1991).
5. Serpone, N., Lawless, D., Disdier, J., and Herrmann, J. M., *Langmuir* **10**, 643 (1994).
6. Sakata, Y., Yamamoto, T., Okazaki, T., Imamura, H., and Tsuchiya, T., *Chem. Lett.* 1253 (1998).
7. Xu, Y., and Langford, C. H., *J. Phys. Chem.* **101**, 3115 (1997).
8. Rey, F., Sankar, G., Maschtmeyer, T., Thomas, J. M., Bell, R. G., and Greaves, G. N., *Top. Catal.* **3**, 121 (1996).
9. Corma, A., Fornes, V., Navarro, M. T., and Perez-Pariente, J., *J. Catal.* **148**, 569 (1994).
10. Davydov, L., Smirniotis, P. G., and France, P., "Photocatalytic Degradation of Organic Compounds," patent application, Procter & Gamble Case 8197 (2001).
11. Sayari, A., Liu, P., Kruk, M., and Jaroniec, M., *Chem. Mater.* **9**, 2499 (1997).
12. Willi, R., Maciejewski, M., Gobel, U., Koppel, R. A., and Baiker, A., *J. Catal.* **166**, 356 (1997).
13. Davydov, L., Smirniotis, P. G., and Pratsinis, S. E., *Ind. Eng. Chem. Res.* **38**, 1376 (1999).
14. Davydov, L., and Smirniotis, P. G., *J. Catal.* **191**, 105 (2000).
15. Carvalho, W. A., Wallu, M., and Schuchardt, U., *J. Mol. Catal. A* **144**, 91 (1999).
16. Karakitsou, K. E., and Verykios, X. E., *J. Phys. Chem.* **97**, 1184 (1993).
17. Litter, M. I., and Navio, J. A., *J. Photochem. Photobiol. A* **84**, 183 (1994).
18. Hoffmann, M. R., Hua, I., and Hochemer, R., *Ultrason. Sonochem.* **3**, S163 (1996).
19. Zhu, Z. D., Chang, Z. X., and Kevan, L., *J. Phys. Chem. B* **103**, 2680 (1999).
20. Ulagappan, N., and Rao, C. N. R., *Chem. Commun.* 1047 (1996).
21. Maciejewski, M., Kohler, K., Schneider, H., and Baiker, A., *J. Solid State Chem.* **119**, 13 (1995).
22. Uhm, J. H., Shin, M. Y., Zhidong, Z., and Chung, J. S., *Appl. Catal. B* **22**, 293 (1999).
23. Zhu, Z., Hartmann, M., Maes, E. M., Czernuszewicz, R. S., and Kevan, L., *J. Phys. Chem. B* **104**, 4690 (2000).
24. Reddy, B. M., Chowdhury, B., Reddy, E. P., and Fernandez, A., *J. Mol.Catal. A* **162**, 431 (2000).
25. Reddy, B. M., Ganesh, I., and Reddy, E. P., *J. Phys. Chem. B* **101**, 1769 (1997).
26. Imamura, I., Ishida, S., Taramoto, H., and Saito, Y., *J. Chem. Soc. Faraday Trans.* **89**, 27 (1993).
27. Pradier, C. M., Rodrigues, F., Marcus, P., Landau, M. V., Kaliya, M. L., Gutman, A., and Herskowitz, M., *Appl. Catal. B* **27**, 73 (2000).
28. Koepke, C., Wisniewski, K., Grinberg, M., Majchrowski, A., and Han, T. P. J., *J. Phys: Condens. Matter* **13**, 2701 (2001).
29. Yamashita, H., Yoshizawa, K., Ariyuki, M., Higashimoto, S., Che, M., and Anpo, M., *Chem.Commun.* 435 (2001).
30. Zang, L., Lange, C., Abraham, I., Storck, S., Maier, W., and Kisch, H., *J. Phys. Chem. B* **102**, 10765 (1998).
31. Hoffmann, M. R., Martin, S. T., Choi, W., and Bahnemann, D. W., *Chem. Rev.* **95**, 69 (1995).